Particle Accelerators, 1991, Vol. 35, pp. 43–51
Reprints available directly from the publisher
Photocopying permitted by license only

THREE-DIMENSIONAL NONLINEAR TRANSVERSE BEAM DYNAMICS OF A RADIO-FREQUENCY QUADRUPOLE: COMPARISON OF PARMTEQ WITH AN EXACT SPACE-CHARGE/IMAGE-CHARGE CALCULATION*

B. D. MURPHY, J. H. WHEALTON, R. J. RARIDON, K. E. ROTHE, W. R. BECRAFT**, and P. M. RYAN

Oak Ridge National Laboratory, P.O. Box 2008, Oak Ridge, Tennessee, 37831.

(Received March 5, 1990)

A small section of a radio-frequency quadrupole accelerator has been analyzed using both a full three-dimensional (3-D) beam-dynamics code and a more conventional beam-dynamics-analysis approach represented by the code PARMTEQ. The computational details of the 3-D approach are outlined. Transverse beam-dynamics effects are compared as they were predicted by both approaches, and the differences between the approaches are shown as a function of beam current. For beam currents in excess of about 100 mA, our results indicate that space-charge/image-charge effects should be treated with detailed calculations.

1. INTRODUCTION

When high-current beams are transported in a radio-frequency quadrupole (RFQ) channel the effect of space charge and image charge are of considerable importance. In a beam-dynamics analysis, the incorporation of space-charge calculations adds to the computational effort and, in fact, a treatment of these phenomena is often deemed prohibitive. A proper accounting of the effects of space charge requires a three-dimensional (3-D) treatment of a set of Vlasov–Poisson (V–P) equations. Most beam-dynamics codes execute considerably simpler calculations, and for currents measured in the tens of milliamperes, the simplifications are often quite appropriate. However, when designing a device to transport currents on the order of an ampere,[1,2] space charge effects assume major importance. The work reported here is a comparison between two kinds of calculations; one group involves a simple and conventional 2-D treatment of space charge, neglecting image charges, whereas the second group of calculations includes image charges in a 3-D V–P formulation. The results of these comparisons will indicate the limitations associated with the simpler approach to the problem.

* Research sponsored by the Exploratory Studies Program of the Oak Ridge National Laboratory, operated for the United States Department of Energy by Martin Marietta Energy Systems, Inc., under contract DE-AC05-840R21400.

** Grumman Space Systems, P.O. Box 3056, Oak Ridge, TN, 37831.

2. BEAM DYNAMICS CALCULATIONS

A conventional approach to beam-dynamics calculations in an RFQ is represented by the analysis in PARMTEQ[3]. In this analysis, space charge is accounted for by a single perturbation of all particle trajectories once per axial interval. This perturbation is determined by calculating the field resulting from the distribution of particles at a point in time during a cycle. The approach is an approximation; it does not continuously calculate the space-charge forces on each particle resulting from the presence of all the other particles, nor are the nonlinear space-charge forces determined self-consistently. It also assumes azimuthal uniformity. However, for many applications this simplified approach may be sufficient.

A 3-D treatment is much more complicated. The more detailed of the approaches reported in this study involves a set of time-dependent V–P equations. This approach has been described by Whealton *et al.*[4–7] It will be compared with calculations using the PARMTEQ analysis. The 3-D approach is described by the following equations:

$$\frac{\partial f(\mathbf{r}, \mathbf{v}, t)}{\partial t} + \mathbf{v} \cdot \nabla f(\mathbf{r}, \mathbf{v}, t) + \frac{q}{m} \nabla \phi(\mathbf{r}, t) \cdot \nabla_{\mathbf{v}} f(\mathbf{r}, \mathbf{v}, t) = 0, \tag{1}$$

$$\nabla^2 \phi(\mathbf{r}, t) = -4\pi \int f(\mathbf{r}, \mathbf{v}, t)\, d\mathbf{v}, \tag{2}$$

$$\Phi(s_n, t) = \Phi_n(t), \qquad n = 0, 1, 2, \ldots, N. \tag{3}$$

Equation (1) is the Vlasov equation and Eq. (2) is Poisson's equation; both are to be solved subject to the boundary conditions in Eq. (3). The Vlasov equation represents the evolution of an ion-distribution function $f(\mathbf{r}, \mathbf{v}, t)$, subject to its inertia and to the time-dependent electric fields. If one starts with Liouville's equation, the Vlasov equation follows when one expresses the momentum time derivatives in terms of the external fields.[8] Equations (2) and (3) indicate the causes of these fields. A set of prescribed surfaces having time-dependent Dirichlet boundary conditions on the potentials would be one cause of these fields. In the limit of a zero-current beam, these boundary conditions would be the only cause of the fields; the right-hand side of Eq. (2) would be zero, and only a Laplace equation would remain. However, the presence of the ion space charge requires the inclusion of the term on the right-hand side of Eq. (2).

Much of the physics of RFQs can be studied without the inhomogeneous term in Eq. (2). Besides the basic linear physics of bunching, acceleration, and betatron and synchrotron oscillations, many other phenomena can be studied. For instance, one can study emittance growth, beam halo, coherent oscillations from misalignment, vane-voltage nonuniformity, and aberrant intervane phase. One can also study vane shape effects and nonuniform beam effects by including the inhomogeneous term in Eq. (2). Arbitrary nonlinear space-charge effects can be considered, and one can study accurately the compromise between space charge and emittance growth in an RFQ. One can also study RFQ end effects, beam scrapers, novel geometries, and multiple-beam funneling. Specifically, the funneling scheme of Stokes and Minerbo[9] or Krejcik[10] could, perhaps, be validated and rms emittance growth determined.

Two phenomena are not described by Eqs. (1–3). First, the vane voltages (for an RFQ) must be specified; they are not calculated. One could go a level deeper and solve the relevant Maxwell equations accounting for the 3-D cavity modes—in particular, the dipole modes known to be present to some extent. An investigation along these lines is under way. Second, Eqs. (1–3) neglect all relativistic effects. The ion-space-charge waves propagate at infinite velocity, and the charges on the metallic surfaces (if assumed perfectly conducting) react to the ion beam instantaneously. No wake fields are produced by the finite transit time of electromagnetic waves.

3. SOLVING THE 3-D PROBLEM

As an overview of the approach used to solve the V–P system of equations, seven steps are described. Many of the details can be found in the references cited.

Step 1. The Poisson equation is considered. For this pass, the source terms are set to zero and a Laplace equation is solved by successive over-relaxation, finite differences, and boundary interpolation within a cell. Considering the desirability of (1) resource utilization and (2) accuracy, iteration reduces memory requirements, contributing to resource utilization, and boundary interpolation contributes to the accuracy per cell. Generally, individual convergence of the solutions is not warranted on each pass because the iteration procedure lends itself to incomplete convergence of the intermediate solutions. Furthermore, the evidence seems to show that the finite-difference method, compared with the finite-element method, improves resource utilization by about a factor of 20 for a Poisson solution of the required accuracy.[11–14] Boundary data for arbitrarily shaped metal surfaces including image charges can be specified as time-dependent Dirichlet conditions. Neumann boundary conditions can also be specified.

Step 2. The Vlasov equation is solved for an arbitrary initial condition using the solution to the Laplace equation above for a time step dt. This technique achieves significant advances in both resource utilization and accuracy.[14–17] Some of this work[15–17] reports a speedup in the Vlasov solver by a factor of 10 over that reported previously[18–20] while at the same time improving the accuracy by over a factor of 10. A finite difference approach[14] reports an improvement by a factor of 400 over previous work[11–13] while still having the same accuracy. The trivial relationship between the coordinates inside an element and the global elements for the uniform Cartesian grid used in this algorithm allows a factor of 20 (of the 400) savings in the Vlasov solver over that employed using irregular elements.[11–13] The Vlasov solver is made self-regulating in accuracy; trajectory refinement is undertaken only in those places that need it.[15–17]

Step 3. The space-charge calculation is done in three dimensions by interpolation over the grid and is infinitely improvable in the sense that, as the 3-D grid is made finer and the number of trajectories is increased, a result as accurate as desired can be obtained. Notice that nowhere is any paraxial-like assumption made, and the fields "to all orders" are directly calculated. Therefore, all aberrations are directly computed. Other nonlinear optics effects computed include space charge and image

charges "to all orders" caused by nonuniform beam density and/or boundaries. (Boundaries also cause nonlinear space-charge forces because they alter the dependence of Φ on r that is required for linearity.)

Step 4. The beam charge is taken as an inhomogeneous term to the Laplace equation solved in step 1. The techniques used in these 3-D codes can, in fact, be used to solve for the more difficult case in which a plasma is present (i.e., an ion distribution, together with an equilibrium distribution of electrons, balancing out the space charge of the ions). This more complex situation adds another inhomogeneous term to Eq. (2). It has been reported on elsewhere[18–20] but is not employed for the current work.

Step 5. The time is moved back by dt, the ions are moved back to their phase-space positions at that time, and the Vlasov equation is again solved using the new fields computed from the Poisson equation solution of step 4. The trajectories are different from those computed in step 2 because of the presence of the space-charge terms (steps 3 and 4).

Step 6. Because the trajectories of step 5 are different from those of step 2; steps 3, 4, and 5 are repeated until there is negligible change. This completes the convergence procedure, and the process advances to the next time step. However, one should note the implication of the iteration consisting of steps 5 and 6.

Step 7. The time is advanced by dt, and steps 2 through 6 are repeated. Thus, beam evolution through the device under consideration is simulated.

4. SIMPLE RADIO-FREQUENCY QUADRUPOLE

Figure 1 illustrates the configuration that was studied—a single cell of an RFQ. The quadrupole vanes do not have undulations; thus, there is no acceleration of the beam. It is not our intent to study the beam while it is being accelerated, but rather to examine the space-charge/image-charge forces as they affect the transverse behavior of the beam. We will describe the analysis of situations in which a square beam pulse of atomic mass 1 is injected with an energy of 100 keV. The quadrupole is driven at 200 MHz, and the peak intervane voltage is 10 kV. The dimensions of the system are described in Fig. 1. For the purpose of these discussions, the z-axis represents the beam axis and the x and y axes point toward the pole tips.

The square simulated beam entering the device is composed of arrays of 16×16 particles in the x–y plane. There are 12 of these arrays in an rf period. This square beam (0.34 cm. $\times$ 0.34 cm. in cross section) is centered on the z axis. Thus, this particular beam has zero emittance as it enters the device; it is not intended that it be a matched beam, for instance. The beam samples the rf focusing field for one cell length, and it is spread evenly throughout one rf cycle. Our analyses will determine the influence of space charge on beam divergence.

5. ZERO-CURRENT CASE

In the limit of zero-current beam, there should be agreement between the PARMTEQ and V–P analyses. Figure 2 is a phase-space plot of a zero-current beam as it exits

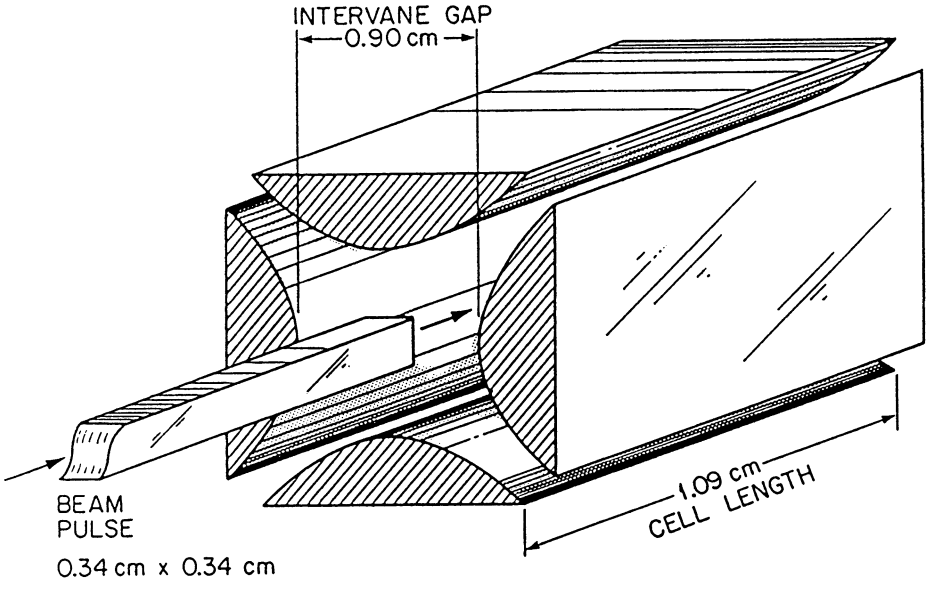

FIGURE 1 A single-cell radio-frequency quadrupole. The energy of the entering beam is 100 keV. The quadrupole is driven at 200 MHz, and the peak intervane voltage is 10 kV.

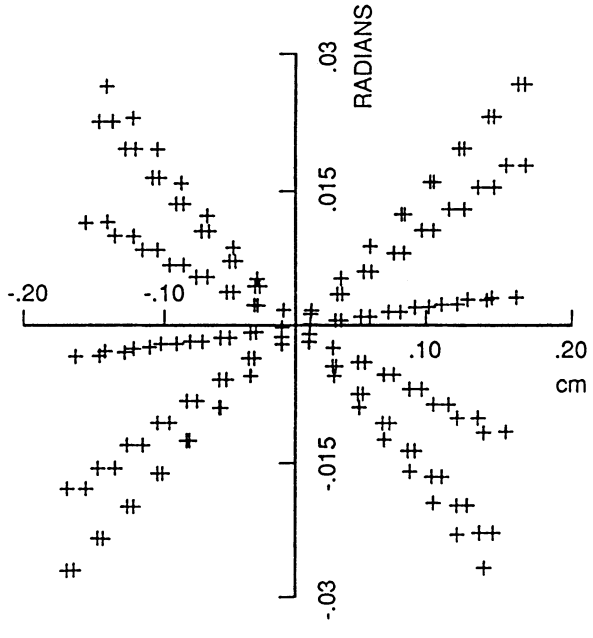

FIGURE 2 The x–x' phase-space plot for a zero-current beam as it exits the quadrupole.

the device. The data displayed in Fig. 2 were obtained as output from PARMTEQ. The results of the V–P analysis are the same.

Figure 2 is an x–x' phase-space plot. A similar plot applies in the y–y' case. The plot shows 12 lines going through the origin and having various slopes, some positive and some negative (two of the lines coincide). Each of these 12 lines corresponds to a group of particles that enter the device at a specific phase of the rf field. The particles in any one group will have various x values, and those having x values indicating a greater distance from the beam axis will suffer a greater (positive or negative) deflection. Each point represents a number of particles having the same x value and phase but having different y values. By definition, a particle's transit time through the cell is one half of an rf cycle. The amount of deflection suffered by a particle will be determined by the integrated value of the field during the transit time interval. Thus, if a particle's transit time interval were centered on an extremum of the field, that particle would suffer a large deflection; if centered on a zero of the field, it would suffer a minimum, or possibly zero, deflection.

6. SPACE-CHARGE EFFECTS

Figure 3 shows a comparison between a PARMTEQ calculation and a V–P calculation when the beam current is 100 mA. Because of the space charge, the convergent

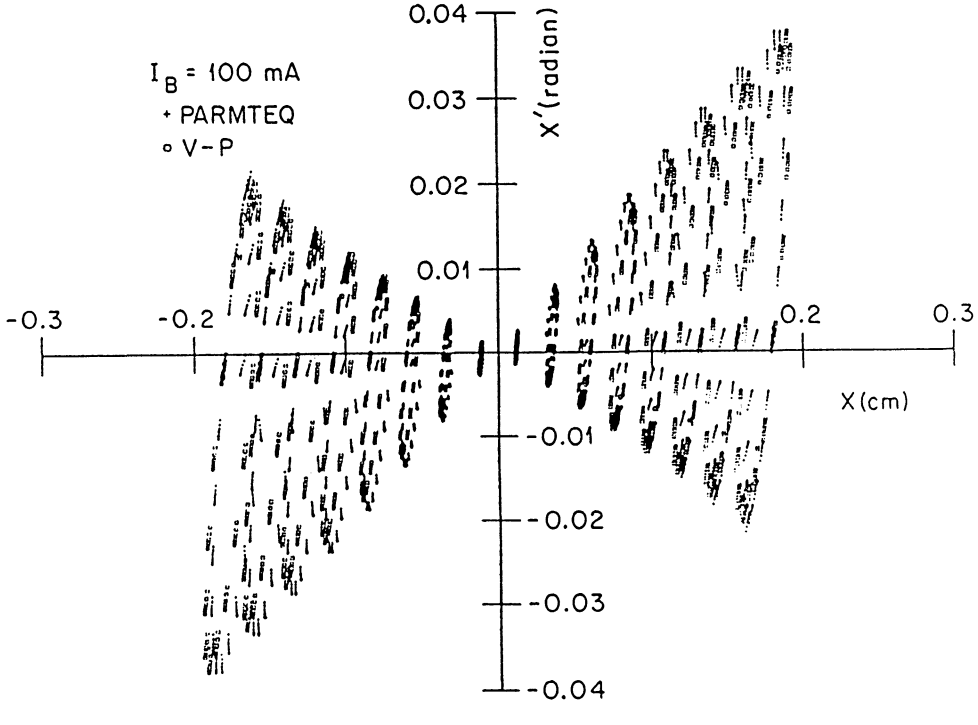

FIGURE 3 Phase-space plots for a 100-mA beam as it exits the quadrupole. Both the PARMTEQ and the 3-D results are shown. A slightly greater transverse motion is predicted by PARMTEQ.

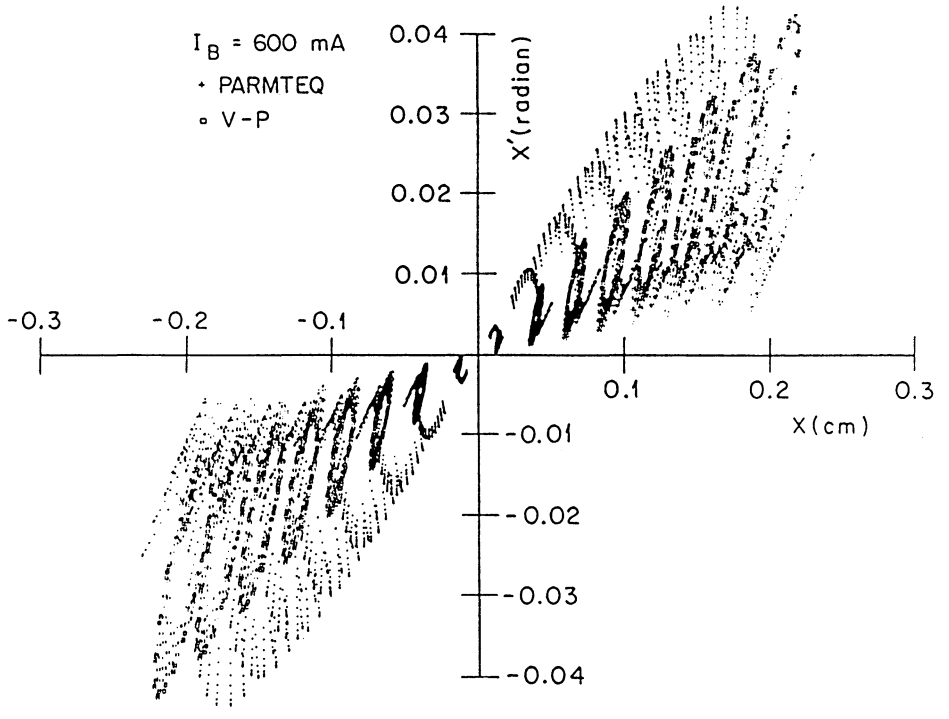

FIGURE 4 Phase-space plots for a 600-mA beam as it exits the quadrupole, showing both PARMTEQ and 3-D results. Again, it can be seen that PARMTEQ predicts more transverse motion than does the 3-D approach. But, in this case, with a larger beam current the difference is quite significant.

trajectories are seen to converge less whereas the trajectories that diverge do so at a greater rate. Also, note that those particles having the same x values and different y values are not now coincident as they were in the zero-current case.

According to Fig. 3, both calculations predict fairly similar behavior for the beam but there is a slight difference. The PARMTEQ calculations show somewhat more divergence than the V–P calculations. Figure 4 shows a comparison for 600 mA, and these differences between the two approaches are seen to have increased with current. Consider those particles whose phase is such that they suffer the most divergence. PARMTEQ in all cases predicts a larger value for that maximum divergence than does the V–P approach. In interpreting these results, keep in mind that the calculations we have described in both cases are simulating a continuous current. On the other hand, most practical applications would involve a bunched beam rather than a continuous one. It is quite possible that, for a beam whose average current is 100 mA, the effective local current could be on the order of 400 mA.

The effect of space charge in the beam has been to introduce a transverse velocity which is apparent in the phase-space plots. Figure 5 summarizes the results in terms of transverse velocity versus beam current. The plots in Fig. 5 show transverse velocity in arbitrary units, and thus, in most cases, they can be considered typical of any pair of corresponding trajectories representing the two calculational approaches. As the transverse velocity results show, agreement between these two approaches is within 2% for local currents that are less than 300 mA.

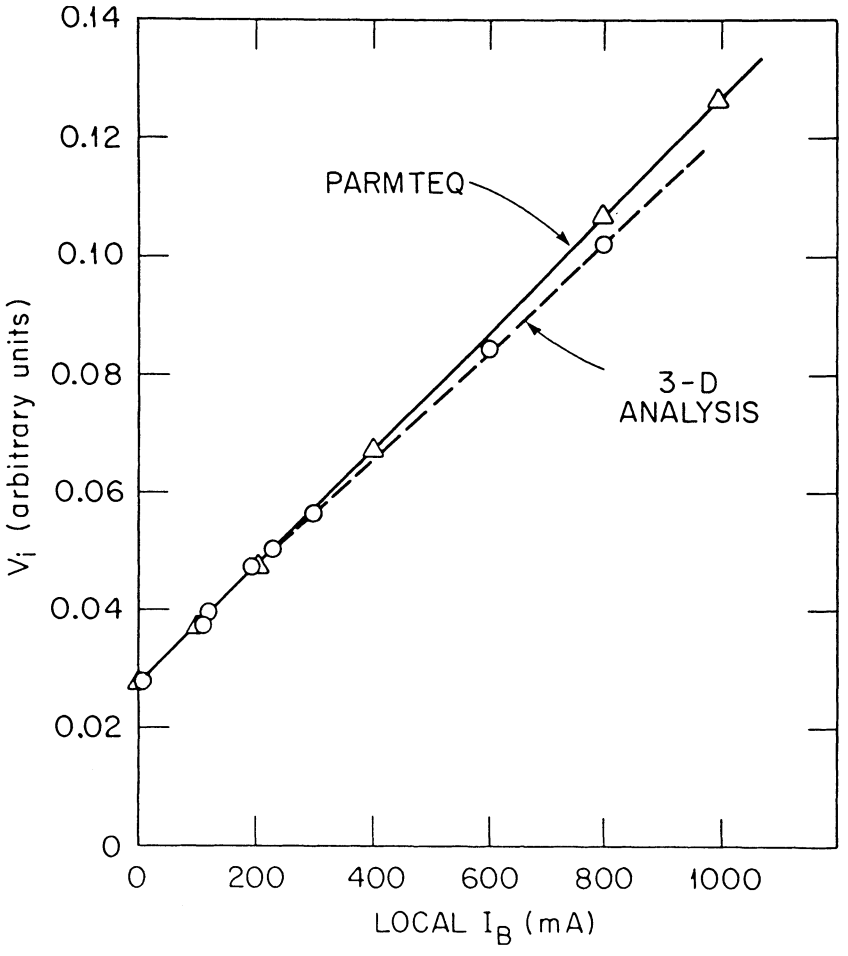

FIGURE 5 A comparison of transverse velocities for a particle orbit both in the case of a PARMTEQ calculation and a full-3-D calculation. These are the calculated transverse velocities at the exit of the quadrupole. The velocity units are arbitrary, meaning that the plot is applicable to most of the orbits.

7. CONCLUSIONS

For the configuration studied and with local currents less than 300 mA there does not appear to be a serious problem when one employs a simple approach in calculating space-charge effects. Therefore, one could say that for a bunched beam up to about 100 mA, the conventional approach to beam-dynamics calculations in an RFQ would seem to be appropriate in the case of the configuration described in Fig. 1. A practical RFQ would be the next device to study in this manner, and it will, undoubtedly, show some more complicated effects. However, the results obtaining for a single cell as a beam drifts through are of fundamental importance, and

they must be first understood because they form the basis with which to disentangle the effects seen in a more complicated device.

Many RFQ designs to date are intended to transport beams that are in the tens of milliamperes. The results reported here do not indicate any severe limitations in the calculation of space-charge effects for such beams. However, with recent interest in very-high-current RFQs[21] that transport some hundreds of milliamperes, it would appear that more accuracy is needed in calculating space-charge effects. Furthermore, as we mentioned in Section 2, it might be profitable to extend the calculations so as to account for the interaction with the rf structure. This could be implemented in the analysis of Whealton *et al.*[22], for instance.

REFERENCES

1. R. H. Stokes, T. P. Wangler, and K. R. Crandall, Proc. IEEE Particle Accelerator Conf., Washington, D.C., March, 1987, p. 334.
2. B. D. Murphy *et al.*, *Nuclear Instruments and Methods*, **A275**, 157 (1989).
3. K. R. Crandall, R. H. Stokes and T. P. Wangler, Proc. of Linear Accelerator Conf., Montauk, N.Y., 1979, p. 205.
4. J. H. Whealton *et al.*, Workshop on Space-Charge Effects in Beam Dynamics, Oak Ridge, Tenn., 1986, IEEE Cat. #87CH2387-9, p. 1057.
5. J. H. Whealton *et al.*, NATO/ASI Meeting on High Brightness Accelerators, Pitlochry, Scotland, 1986.
6. J. H. Whealton *et al.*, Twenty-Eight Annual Meeting of the Division of Plasma Physics, American Physical Society, Baltimore, Md., Nov. 3–7, 1986, and IEEE Particle Accelerator Conference, Washington, D.C., March, 1987, p. 1057.
7. J. H. Whealton *et al.*, in Linear Accelerator and Beam Optics Codes, La Jolla Institute, C. R. Eminhizer, ed., AIP Conf. Proc. 177, 1988, p. 228–260.
8. J. D. Lawson, *The Physics of Charged-Particle Beams*, 2nd Ed., Oxford University Press (1988).
9. R. H. Stokes and G. N. Minerbo, Proceedings of Workshop on High Current, High Brightness and High Duty Factor Ion Injectors, G. H. Gillespie *et al.*, eds., AIP Conf. Proc., **139**, 1985, p. 79.
10. P. Krejcik, Proceedings of Workshop on High Current, High Brightness and High Duty Factor Ion Injectors, G. H. Gillespie *et al.*, AIP Conf. Proc. **139**, 1985, p. 179.
11. J. W. Wooten *et al.*, *J. Comput. Phys.*, **43**, 95 (1981).
12. J. W. Wooten, J. H. Whealton, and D. H. McCollough, *J. Appl. Phys.*, **52**, 6418 (1981).
13. K. Ota *et al.*, *J. Appl. Phys.*, **23**, 1241 (1984).
14. J. H. Whealton, R. W. McGaffey, and P. S. Meszaros, *J. Comput. Phys.*, **63**, 20 (1986).
15. J. H. Whealton, *J. Comput. Phys.*, **40**, 491 (1981).
16. J. H. Whealton, *Nucl. Instrum. Meth.*, **189**, 55 (1981).
17. J. H. Whealton, *IEEE Trans. Nucl. Sci.*, **NS28**, 1358 (1981).
18. J. H. Whealton, E. J. Jaeger, and J. C. Whitson, *J. Comput. Phys.*, **27**, 32 (1978).
19. J. C. Whitson, J. Smith, and J. H. Whealton, *J. Comput. Phys.*, **28**, 408 (1978).
20. J. H. Whealton and J. C. Whitson, *Particle Accelerators*, **10**, 235 (1980).
21. W. R. Becraft *et al.*, Proc. 12th Symp. on Fusion Engineering, Monterey, Calif., 1987, p. 1164.
22. J. H. Whealton *et al.*, *J. Comput. Phys.*, **75**, 168 (1988).